Generation of Entangled-Photons by a Quantum Dot Cascade Source in Polarized Cavities: Using Cavity Resonances to Boost Signals and Preserve the Entanglements

K. Nasiri Avanaki[1, a)] and George C. Schatz[1]

Department of Chemistry, Northwestern University, 2145 Sheridan Road, Evanston IL 60208-3113,USA[b)]

(Dated: 16 March 2023)

Motivated by recent advances in the development of single photon emitters for quantum information sciences, here we design and formulate a quantum cascade model that describes cascade emission by a quantum dot (QD) in a cavity structure while preserving entanglement that stores information needed for single photon emission. The theoretical approach is based on a photonic structure that consists of two orthogonal cavities in which resonance with either the first or second of the two emitted photons is possible, leading to amplification and rerouting of the entangled light. The cavity- QD scheme uses a four-level cascade emitter that involves three levels for each polarization, leading to two spatially entangled photons for each polarization. By solving the Schrodinger equation, we identify the characteristic properties of the system which can be used in conjunction with optimization techniques to achieve the "best" design relative to a set of prioritized criteria or constraints in our optical system. The theoretical investigations include an analysis of emission spectra in addition to the joint spectral density profile, and the results demonstrate the ability of the cavities to act as frequency filters for the photons that make up the entanglements, and to modify entanglement properties. The results provide new opportunities for the experimental design and engineering of on-demand single photon sources.

Keywords: Single photon source, Entangled photon, Polarization, Cascade emission, Cavity hybrid system, Joint spectral density

[a)]Department of Chemistry and Chemical Biology, Harvard University, 12 Oxford Street, Cambridge MA 02138, USA

[b)]Electronic mail: g-schatz@northwestern.edu

I. INTRODUCTION

With the growth of processing capacity doubling every 18 months(or even less), photonic technologies are rapidly growing in importance for secure and reliable information transfer. This has fostered a race to the development and advancement of non-classical light sources: sources that produce photons with controllable quantum correlations. This has resulted in a new scientific frontier where the development of a single-photon emitter (SPE); a fundamental resource for scalable quantum information technologies[1,2], is the main impediment for further progress.

The ideal on-demand SPE radiates exactly one photon at a specified time into a given spatio-temporal mode. Such SPEs play a key role in many proposed quantum computing schemes, including quantum simulation[3], boson sampling[4] , precision measurement[5], quantum memories[6], quantum networks[7] and quantum walks[8]. SPEs are also advantageous or required in variety of quantum secure communication strategies[9]. This great interest in SPEs for cutting-edge quantum technologies has attracted much attention, particularly to its experimental realization in quantum optics[10,11].

The search for 'ideal' on-demand SPEs has led to many promising material systems, and a number of these have progressed beyond proof-of-concept to engineering initiatives, with constantly improved results[12–15].

Recent progress in making SPE's has cleared away some challenges in the nano-fabrication and materials growth techniques, leading to scalable on-chip integration and the fabrication of identical sources[16] for photonic circuits, and using different platforms that include quantum dots(QDs)[17], defects in solids[18], two-dimensional hosts and of course carbon nanotubes[19].

In this work, we consider the decay of an excited QD that emits two photons as a cascade source, leading to entanglement of the two photons. So far, this approach has been examined to produce and measure atomic superposition states[20], generate atom–atom[21] and atom–photon entanglement[22], create single photons[23] and produce entangled photonic states by sequentially manipulating atomic systems[24–26]. In this paper we explore the theoretical foundations of this emission process more rigorously for the case where the emission occurs in a cavity, and we map out the opportunities for achieving useful intensity changes while preserving entanglements for the chosen cavity structure.

The importance of SPEs in different cutting-edge technologies has opened up new research opportunities for enhancing the performance of the system as a single bright source. Taking ad-

vantage of optical microcavities[27,28] in quantum optics and cavity quantum electrodynamics, developments with different geometries (micropillar structures[16,29] , and photonic crystal cavities[30]) have been successfully employed, and these optical resonators have risen in performance and with high fabrication yields either by using the Purcell effect[31,32] or by entering the strong-coupling regime[33].

Comparing monolithic cavities with fixed modes versus open cavities, we see that deterministic fabrication techniques[34,35] have made it possible to carefully design a monolithic cavity-single emitter(SE) hybrid system, matching the spatial and spectral modes between cavity resonances and the emitter. In addition, due to the intrinsic tunability of open cavities, the cavity dimensions can be adjusted to the embedded emitter[36–41]. The latter cases have proven to be a viable method of investigation in cavity quantum electrodynamics (cQED) obtaining the same levels of performance as their monolithic competitors.

It should be noted that in most studies, the cavity's fundamental mode is used, and higher-order modes are so widely separated in frequency that they don't interact with the two-level system. This means when multiple transitions from the same emitter are required for cQED, it's not feasible to design a cavity that uses the fundamental and first-order modes. To circumvent this, two coupled cavities have been combined to create a doublet of hybridized modes[36,42–45]. In order to provide synchronous frequency matching of both modes with multiple transitions from an emitter, this technique necessitates fabrication processing that is much more difficult than for a single-mode cavity.

The cavity- QED implementation used in this paper makes use of a four-level excited QD coupled to two high-Q cavities, which allows for the deterministic generation of polarized-entangled photon pairs (here the Q of a cavity is determined by the energy stored per cycle versus the energy lost. With no absorption by the cavity material, Q is determined by the reflection loss at the interface between the interior and exterior of the cavity). Typically, the generation of correlated photon pairs in semiconductor emitters occurs through a biexciton-exciton cascade emission[16,46,47]. In this process, two electron–hole pairs form a biexciton state that radiatively decays with the emission of two photons in which a single exciton state serves as the intermediate state. This radiative biexciton cascade in a single semiconductor QD provides a source of entangled photons under general circumstances[48–51]. Preparing the QD in a biexciton state often leads to emission of photon pairs with different polarization[52–55].

It should be noted that asymmetry in geometry of the QDs induces splitting of the intermediate

excitonic states, i.e., fine-structure splitting (FSS) (Δ_{FSS}), which is modified as QD size varies. Therefore it is more realistic if we describe our QD biexciton cascade emission using a four-level system composed of a biexciton state ($|B\rangle$), two bright intermediate exciton levels ($|X(Y)\rangle$) with different polarization, and a ground state ($|G\rangle$)[56]. Spontaneous decay of the biexciton state to the ground state thus occurs via two intermediate exciton states leading to the emission of pairs of photons through the transitions $|B\rangle \rightarrow |X(Y)\rangle$ and $|X(Y)\rangle \rightarrow |G\rangle$ respectively (see Fig. 1). Accordingly, the intermediate excitonic states lead to spin-dependent properties in the emission process. Note that the FSS between exciton levels is typically of the order of several tens of μeV[57] and only causes minor quantitative changes to the results, however the entangled polarized photon pairs have a lower degree of entanglement[58,59]. Effective solutions have been presented in past studies[60–65] to resolve this issue so, we ignore it in this work and assume that the two states are degenerate.

In this work, we assume the system is initially (at time; $t = 0$) in the biexciton level $|B\rangle$ with energy $\hbar(\omega_\alpha + \omega_\beta)$ and the lifetime of the two-photon excited state is a parameter that we denote γ_α^{-1}. A second decay rate γ_β is assumed to govern the transition from the exciton state to the ground state. If $\gamma_\alpha \ll \gamma_\beta$, the exciton to ground state emission occurs within a short time delay after the first emission. We have previously demonstrated for emission into vacuum that this leads to a high degree of entanglement of the photons[50,51]. In the present study, we focus on how the cavity alters the emission, with emphasis on the entangled pair that arises when the first photon emitted with one polarization is resonant with the one cavity (cavity 1) while the second photon of that polarization is nonresonant. Another entangled pair arises when both photons have the other polarization, and the first photon is nonresonant while the second photon is resonant with the other cavity (cavity 2, see Fig. 1).

II. THEORY IMPLEMENTATION

The different components of the physical system under investigation are depicted in Fig. 1, including; one four-level QD and two high-Q cavities supporting a single longitudinal mode of angular frequency ω_{c_x} for one cavity and ω_{c_y} for the other, and the two cavities are associated with different polarizations (X and Y), i.e., there are two cavity modes of the electromagnetic (e.m.) field where the optical axes of each cavity are assumed as the quantization axis for the angular momentum. The transitions from biexciton(B) to exciton state(X/Y) and to the ground state(G)

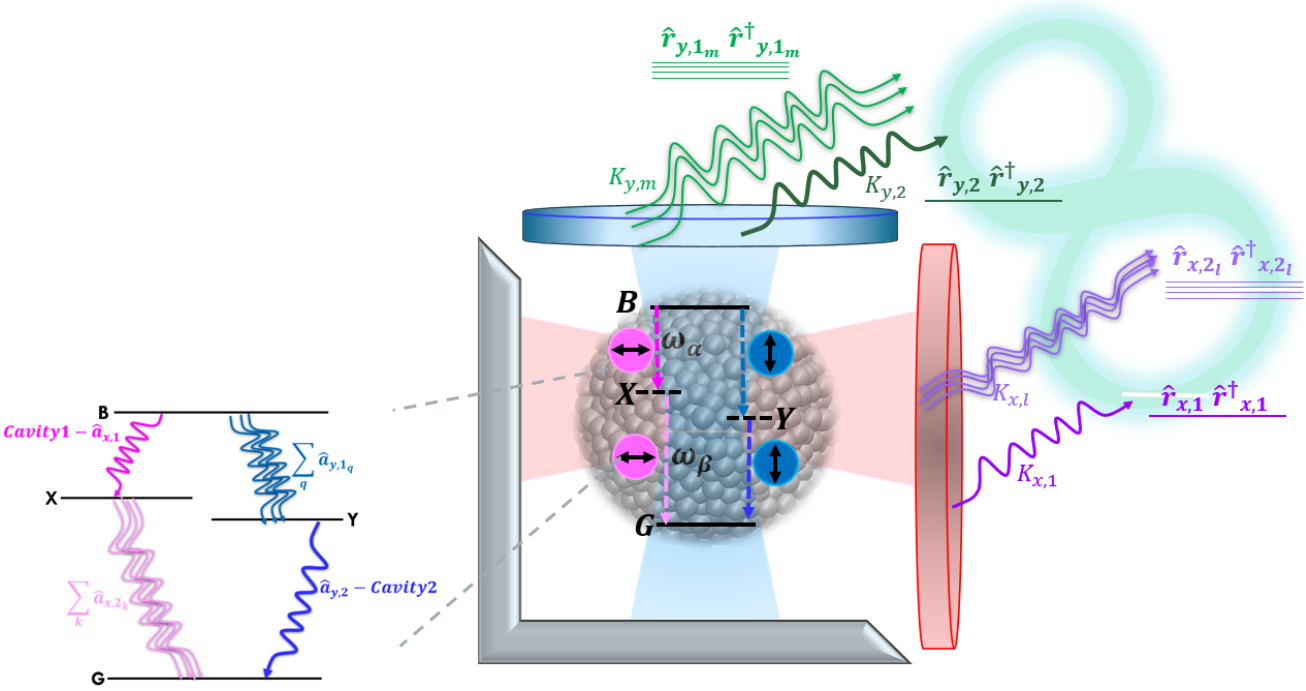

FIG. 1. Four-level system QD that includes: biexciton state ($|B\rangle$), two bright intermediate exciton levels ($|X(Y)\rangle$) with different polarizations, and a ground state ($|G\rangle$) that are coupled to two high-Q cavities with different polarizations. Here the first X- polarized emission ($|B\rangle \rightarrow |X\rangle$) is coupled to cavity 1 and the second Y- polarized emission ($|Y\rangle \rightarrow |G\rangle$) is coupled to cavity 2. Spontaneous decay of the biexciton state to the ground state thus occurs via two intermediate exciton states leading to the emission of pairs of photons through the transitions $|B\rangle \rightarrow |X(Y)\rangle$ and $|X(Y)\rangle \rightarrow |G\rangle$ respectively.

are considered to satisfy the electric dipole selection rules (additional details are provided in our previous work[50,51]), and are coupled to the fundamental optical mode of each cavity.

Here we express the coupled components of our photonic system such as QD, cavity 1, cavity 2 and outside reservoir in mathematical notation, where cavity 1, 2 and outside reservoir are initially in the vacuum states,

$$|QD\rangle \otimes |0_{c_x}\rangle \otimes |0_{c_y}\rangle \otimes |0_{R_x}\rangle \otimes |0_{R_y}\rangle = |QD\rangle \otimes |\Omega\rangle = |QD, \Omega\rangle \tag{1}$$

In the above expression, the first term shows the QD state ($|B\rangle$ or$|X(Y)\rangle$ or$|G\rangle$) coupled (with tensor product) to vacuum states of cavity 1; $\hat{a}_x^{\dagger}(\hat{a}_x)$ and cavity 2; $\hat{a}_y^{\dagger}(\hat{a}_y)$, with $\hat{a}_i^{\dagger}(\hat{a}_i)$ being the photon creation (annihilation) operator in the corresponding cavity mode and then coupled to the outside reservoir; $\hat{r}_{x,y}^{\dagger}(\hat{r}_{x,y})$. Since we assume the QD has initially been excited to the biexciton

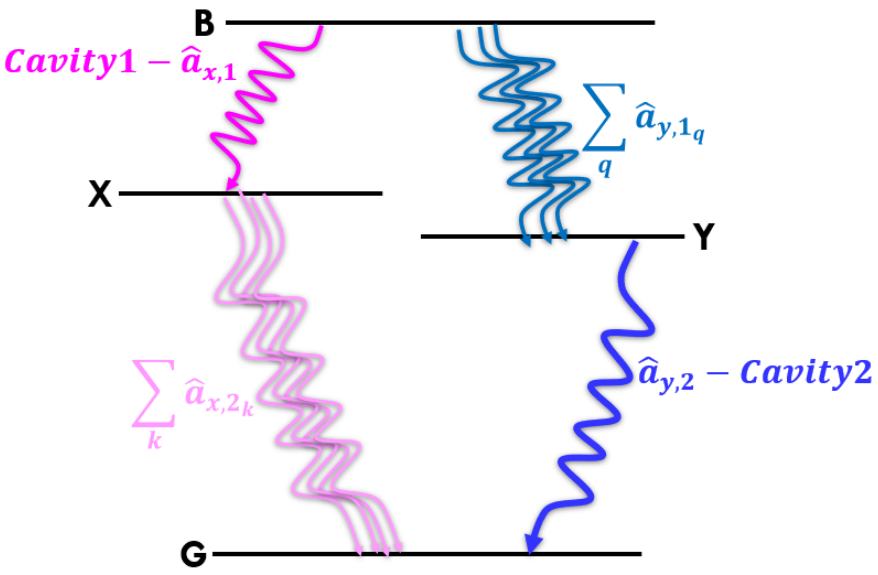

FIG. 2. Emission paths for entangled photon production and the specific coupling with the cavities.

state $|B\rangle$ by another process, the initial state of the whole system at time $t = 0$ is defined as

$$|\psi(t=0)\rangle = |I\rangle = |B,\Omega\rangle \tag{2}$$

We are interested in the describing the near resonant interaction of the QD with the cavity modes. Here we assume the first X- polarized emission ($|B\rangle \rightarrow |X\rangle$) is coupled to cavity 1 and the second Y- polarized emission ($|Y\rangle \rightarrow |G\rangle$) is coupled to cavity 2.

In addition, we assume the right wall of the cavity 1 and the top wall of cavity 2 are partially transparent, so called single-sided Fabry-Perot resonators[66]; that leak photons out to the outside reservoir leading to two entangled photons that can be detected outside of the cavities for single photon applications. The cavity fields, $\widehat{a}_{i=x,y}$ couple to the $\widehat{r}_{i=x,y}$ reservoir oscillator via a coupling constant $g^r_{i=x,y}$ in the rotating-wave approximation. The emissions inside the cavities and the corresponding couplings are depicted in Fig. 2.

The evolution of the whole system is traced by writing down the Hamiltonian governing cavities 1 and 2 and the interactions between 'the QD states and the cavities' and between 'the cavities and the reservoir', including for the two polarization modes. In the following expression, we are considering near-resonant interactions involving quantum dot-cavity interactions, so the biexciton emission of the QD couples specifically to cavity mode x,1 and the exciton emission couples to y,2. Similarly, cavity modes x,1 and y,2 only couple to the corresponding reservoir modes and

there are non-resonant interactions for the other couplings. The resulting Hamiltonian is:

$$\begin{aligned}
\widehat{H}_{cavity} &= \omega_{c_x}\widehat{a}_x^{\dagger}\widehat{a}_x + \omega_{c_y}\widehat{a}_y^{\dagger}\widehat{a}_y \\
\widehat{H}_{QD-cavity} &= g_{\alpha_x}\,\widehat{a}_{x,1}\sigma_{BX}^{\dagger}e^{i(\omega_\alpha-\omega_{c_x})t} + \sum_k g_{\beta_{x,k}}\,\widehat{a}_{x,2_k}\sigma_{XG}^{\dagger}e^{i(\omega_\beta-\omega_k)t} \\
&\quad + \sum_q g_{\alpha_{y,q}}\,\widehat{a}_{y,1_q}\sigma_{BY}^{\dagger}e^{i(\omega_\alpha-\omega_q)t} + g_{\beta_y}\,\widehat{a}_{y,2}\sigma_{YG}^{\dagger}e^{i(\omega_\beta-\omega_{c_y})t} + h.c. \\
\widehat{H}_{cavity-R_{out}} &= g_{x,1}^{r}\,\widehat{a}_{x,1}^{\dagger}\widehat{r}_{x,1}\,e^{i(\omega_{c_x}-\omega_{x,1})t} + g_{y,2}^{r}\,\widehat{a}_{y_2}^{\dagger}\widehat{r}_{y,2}\,e^{i(\omega_{c_y}-\omega_{y,2})t} \\
&\quad + \sum_{l,k} g_{x_l}^{r}\,\widehat{a}_{x,2_k}^{\dagger}\widehat{r}_{x,2_l}\,e^{i(\omega_k-\omega_l)t} + \sum_{m,q} g_{y_m}^{r}\,\widehat{a}_{y,1_q}^{\dagger}\widehat{r}_{y,1_m}\,e^{i(\omega_q-\omega_m)t} + h.c. \\
\widehat{H}_0^{R_{out}} &= \sum_{j_x}\omega_{j_x}\widehat{r}_{j_x}^{\dagger}\widehat{r}_{j_x} + \sum_{j_y}\omega_{j_y}\widehat{r}_{j_y}^{\dagger}\widehat{r}_{j_y}
\end{aligned} \tag{3}$$

where $\sigma_{BX}^{\dagger} = |B\rangle\langle X|$, $\sigma_{XG}^{\dagger} = |X\rangle\langle G|$ and g_{α_x} and g_{β_x} are QD-cavity coupling strengths for transitions from the biexciton state to exciton and then to the ground state respectively inside the cavity and $g_{x,1}$ and $g_{y,2}$ are the vacuum Rabi couplings of the resonant cavity modes vs. the outside reservoir. We also include the nonresonant couplings here but will neglect them later.

Note that the second index for g, $\widehat{a}$ or $\widehat{r}$ is related to the emission event; for instance the first emission for X-polarization and the second emission for X-polarization: $\widehat{a}_{x,1}$ and $\widehat{a}_{y,2}$. We also define the coupling of y-polarized emission differently than x-polarized emission by introducing a phase $e^{i\phi}$; i.e. $g_{\alpha_y} = g_{\alpha_x}\,e^{i\phi}$ and $g_{\beta_y} = g_{\beta_x}\,e^{i\phi}$ (look at these references for more details [67,68]). As we mentioned earlier the FSS between exciton levels is very small and only causes minor quantitative changes to the results so we assume degenerate intermediate levels; $\omega_{\alpha(\beta)_x} = \omega_{\alpha(\beta)_y}$, by setting $\Delta_{FSS} \approx 0$. Note however that $\omega_\alpha \neq \omega_\beta$ for either x or y.

Using $e^{\alpha A}Be^{-\alpha A} = B + \alpha[A+B] + \frac{\alpha^2}{2!}[A,[A,B]]$, we rewrite the complete form of Hamiltonian $(= \widehat{H}_{QD} + \widehat{H}_{cavity} + \widehat{H}_{QD-cavity} + \widehat{H}_{cavity-R_{out}} + \widehat{H}_0^{R_{out}})$ in the interaction picture,

$$\begin{aligned}
\widehat{V}_I &= g_{\alpha_x}\,\widehat{a}_{x,1}\sigma_{BX}^{\dagger}e^{i(\omega_\alpha-\omega_{c_x})t} + \sum_q g_{\alpha_{y,q}}\,\widehat{a}_{y,1_q}\sigma_{BY}^{\dagger}e^{i(\omega_\alpha-\omega_q)t} + \sum_k g_{\beta_{x,k}}\,\widehat{a}_{x,2_k}\sigma_{XG}^{\dagger}e^{i(\omega_\beta-\omega_k)t} \\
&\quad + g_{\beta_y}\,\widehat{a}_{y,2}\sigma_{YG}^{\dagger}e^{i(\omega_\beta-\omega_{c_y})t} + g_{x,1}^{r}\,\widehat{a}_{x,1}^{\dagger}\widehat{r}_{x,1}\,e^{i(\omega_{c_x}-\omega_{x,1})t} + \sum_{k,l} g_{x_l}^{r}\,\widehat{a}_{x,2_k}^{\dagger}\widehat{r}_{x,2_l}\,e^{i(\omega_k-\omega_l)t} \\
&\quad + \sum_{q,m} g_{y_m}^{r}\,\widehat{a}_{y,1_q}^{\dagger}\widehat{r}_{y,1_m}\,e^{i(\omega_q-\omega_m)t} + g_{y,2}^{r}\,\widehat{a}_{y,2}^{\dagger}\widehat{r}_{y,2}\,e^{i(\omega_{c_y}-\omega_{y,2})t} + h.c.
\end{aligned} \tag{4}$$

where $\omega_\alpha - \omega_{c_x}$ and $\omega_\beta - \omega_{c_y}$ are the QD detunings (which we assume are small) with respect to the cavities. Given this, the state vector of the cavity-QD system at any time t is described by

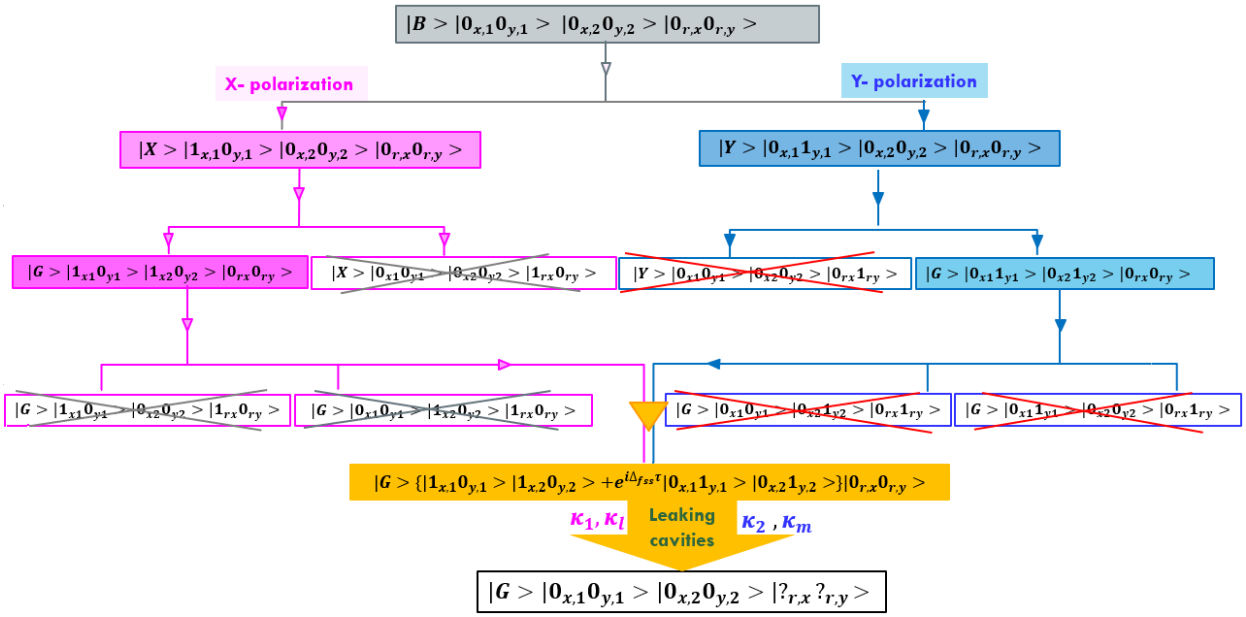

FIG. 3. State notation for different emission paths from biexciton state to the outside reservoir and marking the ones which meet the resonance condition and that we choose to follow for the purpose of this work.

$$
\begin{aligned}
|\psi(t)\rangle = {} & \eta_B(t)\,|B,\Omega\rangle + \eta_X(t)\,\hat{a}^{\dagger}_{x,1}\,|X,\Omega\rangle + \sum_k \eta_k(t)\,\hat{a}^{\dagger}_{x,1}\hat{a}^{\dagger}_{x,2_k}\,|G,\Omega\rangle \\
& + \sum_q \eta_{Y,q}(t)\,\hat{a}^{\dagger}_{y,1_q}\,|Y,\Omega\rangle + \sum_q \eta_q(t)\,\hat{a}^{\dagger}_{y,1_q}\hat{a}^{\dagger}_{y,2}\,|G,\Omega\rangle \\
& + \sum_k \eta^{ox}_k(t)\,\hat{r}^{\dagger}_{x,1}\hat{a}^{\dagger}_{x,2_k}\,|G,\Omega\rangle + \sum_q \eta^{oy}_q(t)\,\hat{a}^{\dagger}_{y,1_q}\hat{r}^{\dagger}_{y,2}\,|G,\Omega\rangle \\
& + \sum_l \eta^{ox}_l(t)\,\hat{r}^{\dagger}_{x,1}\hat{r}^{\dagger}_{x,2_l}\,|G,\Omega\rangle + \sum_m \eta^{oy}_m(t)\,\hat{r}^{\dagger}_{y,1_m}\hat{r}^{\dagger}_{y,2}\,|G,\Omega\rangle
\end{aligned}
\tag{5}
$$

Here, the state vector is a linear combination of the states where the η's are the corresponding slowly varying probability amplitudes. In this expression the last four terms refer to emission of photons to the reservoir modes, so we use the superscript "o" to designate the production of photons "outside" the cavity. Also, the mode labels k and q refer to modes inside the cavity, while l and m refer to modes in the reservoir.

Note that if we define the state vector according to all the emission paths depicted in Fig.3, it would be much more complex, but we selected only the resonant ones with higher probability[53,63,69–71] that are of interest in this work in defining the wavefunction.

We now assume the Wigner-Weisskopf approximation to determine the states of the particle and radiation field as a function of time, where the particle in an excited state decays to the ground state with a characteristic lifetime but does not make back and forth transitions. Then from the

Schrödinger equation $|\dot{\psi}(t)\rangle = -i\widehat{V}_I\,|\psi(t)\rangle$, we construct the equations of motion as:

$$
\begin{aligned}
\dot{\eta}_B(t) &= -ig_{\alpha_x}\, e^{i(\omega_\alpha-\omega_{c_x})t}\eta_X(t) - i\sum_q g_{\alpha_y,q}\, e^{i(\omega_\alpha-\omega_q)t}\eta_{Y,q}(t)\\
\dot{\eta}_X(t) &= -ig^*_{\alpha_x}\, e^{-i(\omega_\alpha-\omega_{c_x})t}\eta_B(t) - i\sum_k g_{\beta_x,k}\, e^{i(\omega_\beta-\omega_k)t}\eta_k(t)\\
\dot{\eta}_{Y,q}(t) &= -ig^*_{\alpha_y,q}\, e^{-i(\omega_\alpha-\omega_q)t}\eta_B(t) - ig_{\beta_y}\, e^{i(\omega_\beta-\omega_{c_y})t}\eta_q(t)\\
\dot{\eta}_k(t) &= -ig^*_{\beta_x,k}\, e^{-i(\omega_\beta-\omega_k)t}\eta_X(t) - ig^{r*}_{x,1}\, e^{-i(\omega_{c_x}-\omega_{x,1})t}\eta^{ox}_k(t)\\
\dot{\eta}_q(t) &= -ig^r_{y,2}e^{i(\omega_{c_y}-\omega_{y,2})t}\eta^{oy}_q - ig^*_{\beta_y}e^{-i(\omega_\beta-\omega_{c_y})t}\eta_{Y,q}\\
\dot{\eta}^{ox}_k(t) &= -ig^{r*}_{x,1}e^{-i(\omega_{c_x}-\omega_{x,1})t}\eta_k - i\sum_l g^r_{x_l}e^{i(\omega_k-\omega_l)t}\eta^{ox}_l\\
\dot{\eta}^{oy}_q(t) &= -ig^{r*}_{y,2}e^{-i(\omega_{c_y}-\omega_{y,2})t}\eta_q - i\sum_m g^r_{y_m}e^{i(\omega_q-\omega_m)t}\eta^{oy}_m\\
\dot{\eta}^{ox}_l(t) &= -i\sum_k g^{r*}_{x_l}e^{-i(\omega_k-\omega_l)t}\eta^{ox}_k\\
\dot{\eta}^{oy}_m(t) &= -i\sum_q g^{r*}_{y_m}e^{-i(\omega_q-\omega_m)t}\eta^{oy}_q
\end{aligned}
\tag{6}
$$

Solving this coupled equations lead to an expression for the amplitude of the outgoing waves as follows (for details see Appendix A):

$$
\eta^{ox}_l \approx -2g^*_{\beta_x}g^*_{\alpha_x}\frac{\kappa_{x_l}}{(\omega_{c_x1}+i\kappa_{x_l})(-i\omega_{\beta l}-i\omega_{c_x1}-i\omega_{\alpha c_x}-\gamma_\alpha)(-i\omega_{\beta l}-i\omega_{c_x1}-\gamma_{\beta x})} \tag{7}
$$

$$
\eta^{oy}_m \approx -g^*_{\beta_y}g^*_{\alpha_y}\frac{\kappa_{y_m}}{(\omega_{c_y2}+i\kappa_{y_m})(-i\omega_{\alpha m}-i\omega_{\beta c_y}-i\omega_{c_y2}-\gamma_\alpha)(-i\omega_{\beta c_y}-\gamma_{\beta_y})} \tag{8}
$$

These are our key results (Eq. 7 and Eq. 8) which show the relationship between scattering amplitudes and properties of the emitter and cavity. Eq. 7 and Eq. 8 allow us to predict and optimize the functionality of our optical system as a SPE. In bellow we use these findings to discuss some aspects of entangled photon generated by Cavity-QD system studied here.

III. APPLICATIONS OF THE THEORY

A. Signature of entangled photons through joint spectral density

As mentioned earlier, advances toward applications of the biexciton structure in a quantum dot as a source of polarized entangled photon pairs are still very attractive[12,13]. Here we show that the entanglement can be preserved while the spectrum of emitted light is modified via cavities.

In the absence of a fine-structure splitting; $\Delta_{FSS} = 0$, the two possible two-photon de-excitation paths without cavities are indistinguishable except for their polarization degree of freedom (x or y), producing equal frequency photon pairs[72]. The non-zero fine-structure splitting provides 'which path' information that impairs indistinguishability, while producing photons that are entangled in both frequency and polarization.

In the present application, the quantum dot is further coupled with cavities, leading to both frequency and polarization entanglement in the emitted photons,

$$|\psi_{EP}\rangle = \frac{1}{\sqrt{2}}\left[\eta^{ox}\,\hat{r}^{\dagger}_{x,1}\hat{r}^{\dagger}_{x,2}\,|G,\Omega\rangle + \eta^{oy}\,\hat{r}^{\dagger}_{y,1}\hat{r}^{\dagger}_{y,2}\,|G,\Omega\rangle\,\right] \tag{9}$$

Given the analytical expressions for the amplitude of our polarized photons in the reservoir, we can examine the existence of entanglement and manipulate the quality of the entanglement as a function of parameters of the model. We performed some computations using parameters that simulate polarization-entangled photon pairs from a biexciton cascade for a single InAs QD embedded in a GaAs/AlAs planar microcavity[73,74]. Here we look at the joint spectral density (JSD) of both photons in the x and y directions, $|\eta^{ox}_{l}|^2$, $|\eta^{oy}_{m}|^2$, respectively (see Fig. 4). The entanglement degree can be varied via the emission bandwidths and other relevant parameters in Eq. 7 and Eq. 8. In practice, the JSD profile can be observed and measured through Hong–Ou–Mandel(HOM) quantum interference experiments which quantifies the two-photon coherence bandwidth and the indistinguishablity of the photon pair[75,76]. Here in Fig. 4, the vertical and horizontal axes show the detunings from the resonant cavity frequencies for x (left panel) and y (right panel)-polarized photon emissions into the reservoir modes from the cavities. We observe that the probability of frequency correlation is the highest in a very short range of detunings close to the resonance conditions: $|\omega_\alpha - \omega_{c_x}| = 0$ for x-polarized and $|\omega_\beta - \omega_{c_y}| = 0$ for y-polarized.

At the same time, the distribution is highly aligned with the anti-diagonal wherein $\omega_\alpha + \omega_\beta = \omega_1 + \omega_l$ and $\omega_\alpha + \omega_\beta = \omega_2 + \omega_m$ for x-polarized photon and y-polarized respectively. For the parameters we have chosen(particularly the cavity frequencies), the bright antidiagonal peak in the x-polarized result is shifted below the (0,0) origin in Fig. 4 by roughly 2 GHz while the y-polarized result is shifted up relative to the (0,0) origin by about the same amount. This detuning arises because the second x-polarized photon and the first y-polarized photon are not in resonance with the cavity.

In addition to the anti-diagonal correlation behavior in both directions, we recognize that the intensity is a few orders of magnitude higher in x-polarized photon emission than in y-polarized.

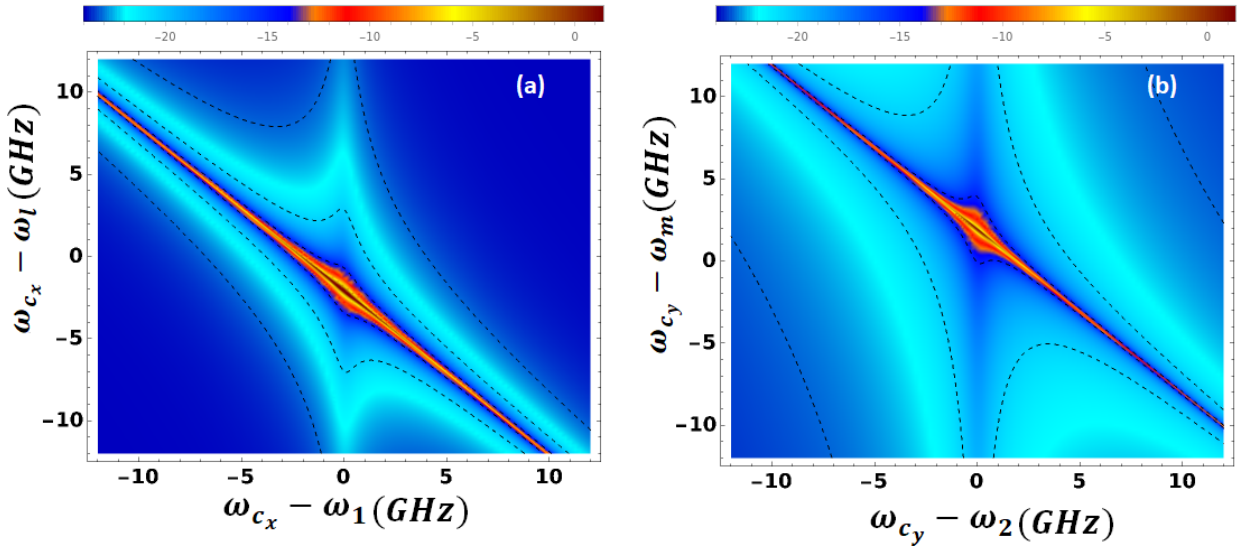

FIG. 4. Panel (a); joint spectral density, $|\eta_l^{ox}|^2$; and Panel (b); $|\eta_m^{oy}|^2$. Using Eq. 7 and Eq. 8, here we assumed $|\omega_\alpha - \omega_{c_x}| = |\omega_\beta - \omega_{c_y}| = 0.05$ GHz which is the near resonance condition between QD and cavities. Other assumptions are: $\omega_\alpha = 1.5$ GHz, $\omega_\beta = 3.5$ GHz, $\phi = \pi/4$, $\gamma_{\alpha_x} = 0.005$ GHz, $\kappa_{x_l} = \kappa_{y_m} = \gamma_{\beta_x} = 0.5$ GHz. The scale bar is logarithmic and the dashed lines(-16 to -6 with stepping of 5) refer to the same intensity scale for X and Y polarization direction.

This reflects differences in the prefactors (the terms that couple the quantum dot to the cavities) in Eq. 7 and Eq. 8. It is also worth mentioning that the dashed lines(contours going from -16 to -6 with a step of 5) in Fig. 4, refer to the same intensity scale for X and Y-polarization directions. We notice that as we tune the frequencies well away from the peak spectral density, the intensity changes more slowly for Y-polarization where it is the second photon that is resonant with the cavity than for X-polarization. However close the the peak of the antidiagonal the width of the peaks measured perpendicular to the antidiagonal are about the same for x and y. This happens because we chose the x and y decay parameters to be the same, i.e., γ_{α_x}=γ_{α_y} and γ_{β_x}=γ_{β_y}. In Appendix B, we show based on our earlier work[51] that this leads to x and y entanglements which are similar. However these parameters can be varied in various ways, such as changing the FSS, so it is possible to adjust the Schmidt numbers of the entanglements using the cavity as well.

It is interesting to compare the results in Fig. 4 with those obtained in the heralding paper[51], where an amplitude analogous to Eq. 7 and Eq. 8 is given by Eq. 10 of that paper;

$$\eta_{\mathbf{kq}}^{cas} = \frac{g_\alpha g_\beta}{(\omega_q - \omega_\beta + i\gamma_\beta)(\omega_k + \omega_q - \omega_\alpha - \omega_\beta + i\gamma_\alpha)}$$

What we find is that the numerator and denominators of Eq. 7 and Eq. 8 have the same structure

as Eq. 10, but with additional terms. The numerator in Eq. 10 involves a product of g_α and g_β, as in Eq. 7 and Eq. 8, but there is an extra factor κ in Eq. 7 and Eq. 8. The denominator in Eq. 10 involves two of the three terms in parenthesis in Eq. 7 and Eq. 8, with the new term involving $(\omega + i\kappa)$. Overall this leads to a factor $\kappa/(\omega + i\kappa)$ in the amplitudes in Eq. 7 and Eq. 8 that is the same on resonance as in Eq. 10 (leaving out some additional refinements that we mention shortly). This suggests that the cavity doesn't enhance the emitted field compared to what comes directly from the quantum dot, as makes physical sense given that the cavity is a passive structure. However the cavity does change a number of factors. It is easy to see from Fig. 4 that the resonance frequencies of the emitted light are determined by the cavity frequencies ω_{cx} and ω_{cy} rather than by the quantum dot frequencies. Another difference arises from the factor $1/(\omega + i\kappa)$ that was just mentioned, as this could lead to a much narrower resonance when $\omega_1 = \omega_{cx}$ in Eq. 7 or when $\omega_2 = \omega_{cy}$ in Eq. 8 than is possible without the cavity. This indicates that the cavity acts in many respects acts a filter that modifies frequencies and amplitudes and entanglements associated with the quantum dot emission while transducing emission to the reservoir photons.

Another issue is what happens if the cavity resonance is narrower than the QD resonance. Here we note that it is the γ_α width that controls the most intense features in Fig. 4. However, one could imagine that if the cavity modes are narrower, such that $\kappa_{xl} < \gamma_\alpha$, then Fig. 4(a) would be dominated by the resonance at $\omega_1 = \omega_{cx}$, rather than the anti-diagonal. This would suppress the entanglement since entanglement requires that the anti-diagonal character be more important. This situation is displayed in Fig. 5, left panel, where the resonance at $\omega_1 = \omega_{cx}$ is more important. In fact the cavity effect is weakened and the system is mildly perturbed by cavity in this case. So, a conclusion from this work is that we need to work in the regime where the cavity resonance is broader than the QD linewidth for the first emitted photon (in x- direction) and second photon emission in the y-direction.

B. One-photon correlation function, $G^{(1)}$

In order to visualize the spectra of the emitted photons, here we look at the one-photon correlation function $G^{(1)}(\tau)$, where an important property of the first-order correlation function is that it forms a Fourier transform pair with the power spectrum expressed as: $S(\omega) = \frac{1}{\pi} Re \int_0^\infty d\tau G^{(1)}(\tau) e^{-i\omega\tau}$. The spectrum is obtained by performing a photon number measurement for a specific mode on a given state, i.e. for a given two-photon state density ρ, its spectrum is

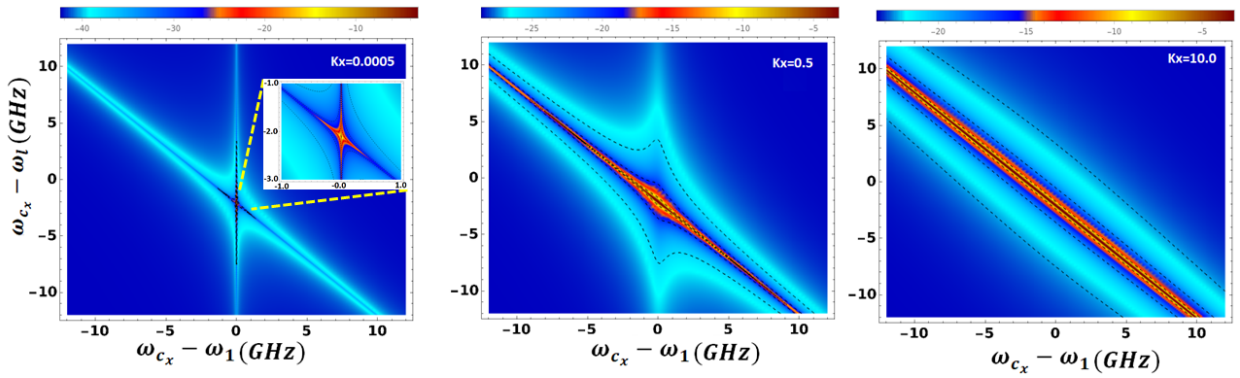

FIG. 5. Joint spectral density, $|\eta_l^{ox}|^2$; here we assumed $|\omega_\alpha - \omega_{c_x}| = 0.05$ GHz where the QD-cavity 1 meets the near resonance condition. Other assumptions are: $\omega_\alpha = 1.5$ GHz, $\omega_\beta = 3.5$ GHz, $\phi = \pi/4$, $\gamma_{\alpha_x} = 0.005$ GHz, $\gamma_{\beta_x} = 0.5$ GHz and $\kappa_{x_l} = 0.0005, 0.5, 10.0$ GHz for the three images. The scale bar is logarithmic.

given by $S(\omega) = \mathrm{Tr}[\hat{a}^\dagger(\omega)\hat{a}(\omega)\rho]$. Using Eq. 7 and Eq. 8 along with residue theorem, for the case where $\gamma_\alpha \ll \gamma_{\beta_{x/y}}$ (this is a good approximation as it was explained in the introduction) with some simplifications we arrive at,

$$G_x^{(1)} = \sum_l |\eta_l^{ox}|^2 \qquad \Rightarrow \qquad S_x \tag{10a}$$

$$\approx |2g_{\beta_x}^* g_{\alpha_x}^*|^2 \frac{\bar{\kappa}_x}{2\gamma_\alpha(\omega_{c_x 1}^2 + \bar{\kappa}_x^2)} \times \frac{1}{(\omega_{\alpha c_x}^2 + \gamma_{\beta x}^2)} \qquad \gamma_\alpha \ll \gamma_{\beta_{x/y}} \tag{10b}$$

$$G_y^{(1)} = \sum_m |\eta_m^{oy}|^2 \qquad \Rightarrow \qquad S_y \tag{10c}$$

$$= |g_{\beta_y}^* g_{\alpha_y}^*|^2 \frac{\bar{\kappa}_y}{2\gamma_\alpha(\omega_{c_y 2}^2 + \bar{\kappa}_y^2)} \times \frac{1}{(\omega_{\beta c_y}^2 + \gamma_{\beta_y}^2)} \tag{10d}$$

Here $\bar{\kappa}_{x,y}$, are the average decay from x- and y-directions. Knowing that[51]; $g_{\alpha_i} g_{\beta_i} \propto \sqrt{\gamma_{\alpha_i}\gamma_{\beta_i}}$ where $i = x, y$, then the total power spectrum is then obtained as follows,

$$S(\omega) = \mathrm{Re}\{G_x^{(1)}(\omega) + G_y^{(1)}(\omega)\} \tag{11}$$

When the resonance condition between QD and cavities are met; $\omega_{\alpha c_x} = 0$ and $\omega_{\beta c_y} = 0$, the spectrum is simplified into Lorentzian line shape functions;

$$\begin{aligned} S_x &= \frac{2\gamma_{\alpha_x}}{\gamma_\alpha \gamma_{\beta x}} \times \frac{\bar{\kappa}_x}{[(\omega_{c_x} - \omega_1)^2 + \bar{\kappa}_x^2]} \qquad \gamma_\alpha \ll \gamma_{\beta_{x/y}} \\ S_y &= \frac{\gamma_{\alpha_y}}{2\gamma_\alpha \gamma_{\beta_y}} \frac{\bar{\kappa}_y}{[(\omega_{c_y} - \omega_2)^2 + \bar{\kappa}_y^2]} \end{aligned} \tag{12}$$

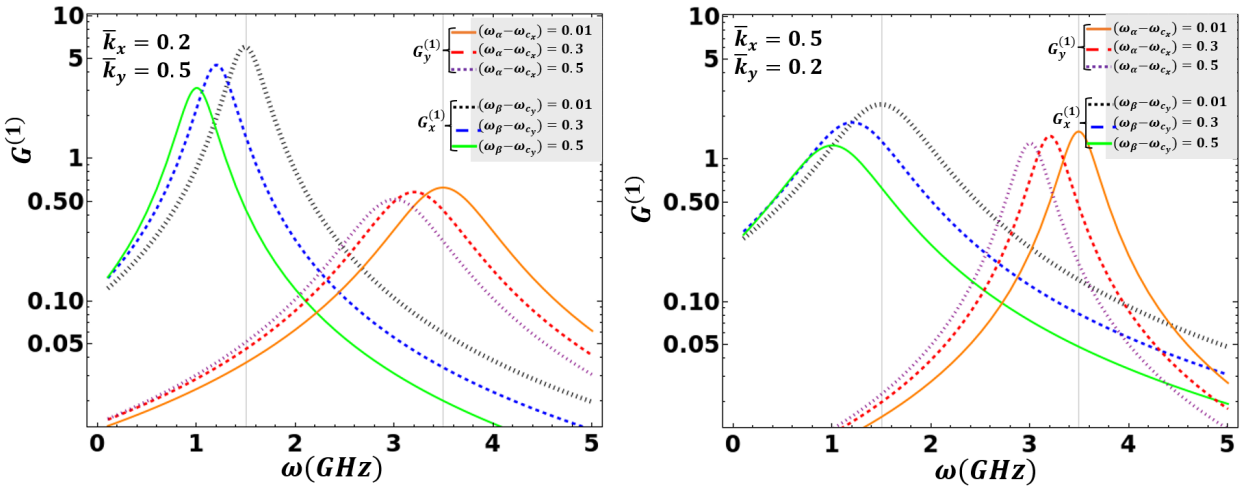

FIG. 6. The total power spectrum $S(\omega)$ in near resonance condition vs. $\omega = \omega_{1,2}$ for X- and Y- polarization. Here $\omega_\alpha = 1.5$ GHz, $\omega_\beta = 3.5$ GHz, $\phi = \pi/4$, $\gamma_{\alpha_x} = 0.005$ GHz, $\gamma_{\beta_x} = 0.5$ GHz.

We notice that the line shape broadening in the above spectra is determined by decay of the cavities in x- and y- directions, $\bar{\kappa}_x$ and $\bar{\kappa}_y$, and this can be seen in the plotted power spectra (for both x- and y- emissions) in different scenarios when the resonance condition is changed (see Fig. 6). Furthermore, when decay of the cavities varies, the plots indicate that the choices of cavity decay factor are reflected in a phenomenological linewidth for the emissions. However the height of the spectra fluctuate as an intrinsic property of the QD as γ_α and γ_β differ. Also note that the results illustrate that the peak of spectra red shift (moving to lower frequency) as the QD is stepped away from the resonance condition in both x- and y-polarized spectra.

C. Probability of polarized emissions into the reservoir

Another interesting analysis can be done by looking at the total amplitude in both x and y direction and in all frequencies,

$$\begin{aligned} A^x_{SPE} &= \sum_l \eta^{ox}_l = -\sum_l 2g^*_{\beta_x} g^*_{\alpha_x} \frac{\kappa_{x_l}}{(\omega_{c_x1} + i\kappa_{x_l})(-i\omega_{\beta l} - i\omega_{c_x1} - i\omega_{\alpha c_x} - \gamma_\alpha)(-i\omega_{\beta l} - i\omega_{c_x1} - \gamma_{\beta x})} \\ &\propto -2g^*_{\beta_x} g^*_{\alpha_x} \frac{\bar{\kappa}_x}{(\omega_{c_x1} + i\bar{\kappa}_x)[\omega_{\alpha c_x} + i(\gamma_{\beta x} - \gamma_\alpha)]} \end{aligned} \tag{13}$$

$$\begin{aligned} A^y_{SPE} &= \sum_m \eta^{oy}_m = -\sum_m g_{\beta_y} g^*_{\alpha_y} \frac{\kappa_{y_m}}{(\omega_{c_y2} + i\kappa_{y_m})(-i\omega_{\alpha m} - i\omega_{\beta c_y} - i\omega_{c_y2} - \gamma_\alpha)(-i\omega_{\beta c_y} - \gamma_{\beta_y})} \\ &\propto -ig_{\beta_y} g^*_{\alpha_y} \frac{\bar{\kappa}_y}{(\omega_{c_y2} + i\bar{\kappa}_y)(\omega_{\beta c_y} - i\gamma_{\beta_y})} \end{aligned}$$

The probability of emission outside of the cavity is

$$\begin{aligned} P_{SPE} &= P^x_{SPE} + P^y_{SPE} = |A^x_{SPE}|^2 + |A^y_{SPE}|^2 \\ &= \frac{4\gamma_{\beta_x}\gamma_{\alpha_x}\bar{\kappa}^2_x}{(\omega^2_{c_x1} + \kappa^2_{x_l})[\omega^2_{\alpha c_x} + (\gamma_{\beta x} - \gamma_\alpha)^2]} + \frac{\gamma_{\beta_y}\gamma_{\alpha_y}\bar{\kappa}^2_y}{(\omega^2_{c_y2} + \kappa^2_{y_m})(\omega^2_{\beta c_y} + \gamma^2_{\beta_y})} \end{aligned} \tag{14}$$

The probabilities of x- and y- polarized emission; P^x_{SPE}, P^y_{SPE} are plotted in Fig. 7. These indicate that the x-polarized emission is red-shifted respect to y-polarized emission. This seems reasonable since the most intense emission happens when the system is in near resonance with the first cavity. However for the y- polarized emission the most intense emission (less intense compared with the x-polarized emission) occurs when the near resonance condition with the second cavity is met. It should be noted that in this work, we assumed that the coupling strength between the QD and cavities is constant, however in general it depends on the position of the QD inside the cavity. In a simplest model, the coupling can be defined as $g_{c_x}(z) = g_{c_x}\cos(2\pi z/\lambda_{c_x})$. In this expression the position z is with respect to the left wall of the cavity 1, and λ_{c_x} is the wavelength of the cavity mode (the corresponding angular frequency is $\omega_{c_x} = 2\pi c/\lambda_{c_x}$)[77]. In the same fashion we can define the distance dependence of the QD position respect to the bottom wall of cavity 2, assuming the detectors are located at the right and top of the system respectively. This is another degree of freedom that can be manipulated to achieve high intense emission at the reservoir in both x and y directions.

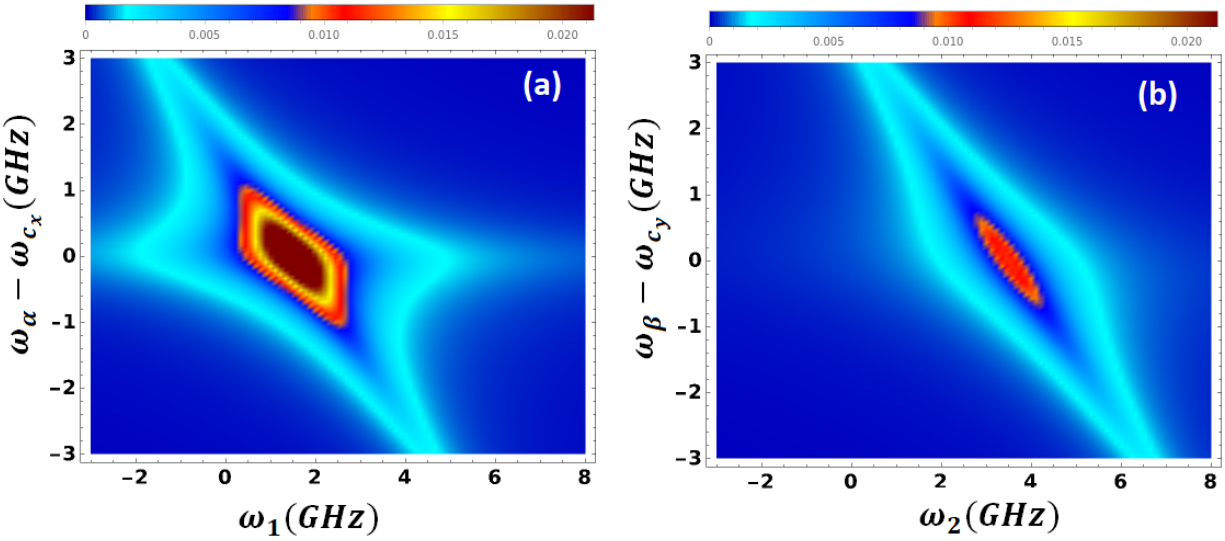

FIG. 7. (a) Probability of X- and (b) Y- polarization emissions; P^x_{SPE}, P^y_{SPE} respectively. Using Eq. 14, we assumed $\phi = \pi/4$, $\gamma_{\alpha_x} = 0.005$ GHz, $\bar{\kappa}_x = \bar{\kappa}_y = \gamma_{\beta_x} = 0.5$ GHz.

IV. CONCLUSION

In conclusion, in this work we derived comprehensive analytical formulas to investigate the emission spectra of entangled photons in a QD-cavity coupled system. Solving the Schrodinger equation, we traced the creation of the radiated photons into the reservoir and we characterized the results by examining the JSD and spectra. By examining the amplitudes of the emissions in both x and y directions, we were able to predict the best case scenarios for producing highly entangled bright photons. The emission can be significantly modified by coupling to the cavities, with resonant frequencies that are determined by the cavity resonances rather than the quantum dots, but the maximum resonant amplitude for emission is the same. The entanglements are also maintained in some limits, which is important for secure information transfer in communication technology. These theoretical investigations and the analysis provide a backbone for the experimental design and engineering of an on-demand single photon source. One can therefore modify the entangled photon properties and the performance of the single-photon properties by optimizing the characteristic parameters of the system using our analytical formulations.

ACKNOWLEDGMENTS

The cavity research was supported as part of the Center for Molecular Quantum Transduction, an Energy Frontier Research Center funded by the U.S. Department of Energy (DOE), Office of Science, Basic Energy Sciences (BES), under Award DE-SC0021314 for cavity properties. Cascade emission properties were supported by NSF grant CHE-2055565. This research was also supported in part through the computational resources and staff contributions provided for the Quest high-performance computing facility at Northwestern University, which is jointly supported by the Office of the Provost, the Office for Research, and Northwestern University Information Technology.

Appendix A: Solving the equations of motion

As explained in the main text, from the Schrödinger equation $|\dot{\psi}(t)\rangle = -i\widehat{V}_I\,|\psi(t)\rangle$ and the state vector, we construct the equations of motion as:

$$
\begin{aligned}
\dot{\eta}_B(t) &= -ig_{\alpha_x}\, e^{i(\omega_\alpha-\omega_{c_x})t}\,\eta_X(t) - i\sum_q g_{\alpha_y,q}\, e^{i(\omega_\alpha-\omega_q)t}\,\eta_{Y,q}(t)\\
\dot{\eta}_X(t) &= -ig^*_{\alpha_x}\, e^{-i(\omega_\alpha-\omega_{c_x})t}\,\eta_B(t) - i\sum_k g_{\beta_x,k}\, e^{i(\omega_\beta-\omega_k)t}\,\eta_k(t)\\
\dot{\eta}_{Y,q}(t) &= -ig^*_{\alpha_y,q}\, e^{-i(\omega_\alpha-\omega_q)t}\,\eta_B(t) - ig_{\beta_y}\, e^{i(\omega_\beta-\omega_{c_y})t}\,\eta_q(t)\\
\dot{\eta}_k(t) &= -ig^*_{\beta_x,k}\, e^{-i(\omega_\beta-\omega_k)t}\,\eta_X(t) - ig^{r*}_{x,1}\, e^{-i(\omega_{c_x}-\omega_{x,1})t}\,\eta^{ox}_k(t)\\
\dot{\eta}_q(t) &= -ig^r_{y,2}e^{i(\omega_{c_y}-\omega_{y,2})t}\,\eta^{oy}_q - ig^*_{\beta_y}e^{-i(\omega_\beta-\omega_{c_y})t}\,\eta_{Y,q}\\
\dot{\eta}^{ox}_k(t) &= -ig^{r*}_{x,1}e^{-i(\omega_{c_x}-\omega_{x,1})t}\,\eta_k - i\sum_l g^r_{x_l}e^{i(\omega_k-\omega_l)t}\,\eta^{ox}_l\\
\dot{\eta}^{oy}_q(t) &= -ig^{r*}_{y,2}e^{-i(\omega_{c_y}-\omega_{y,2})t}\,\eta_q - i\sum_m g^r_{y_m}e^{i(\omega_q-\omega_m)t}\,\eta^{oy}_m\\
\dot{\eta}^{ox}_l(t) &= -i\sum_k g^{r*}_{x_l}e^{-i(\omega_k-\omega_l)t}\,\eta^{ox}_k\\
\dot{\eta}^{oy}_m(t) &= -i\sum_q g^{r*}_{y_m}e^{-i(\omega_q-\omega_m)t}\,\eta^{oy}_q
\end{aligned}
\tag{A1}
$$

We next rearrange the above equations according to Wigner-Weisskopf approximation and follow our previous work[51] as,

$$\begin{aligned}
-ig_{\alpha_x}\, e^{i(\omega_\alpha-\omega_{c_x})t}\,\eta_X(t) &= -\gamma_{\alpha_x}\,\eta_B(t)\\
-i\sum_q g_{\alpha_y,q}\, e^{i(\omega_\alpha-\omega_q)t}\,\eta_{Y,q}(t) &= -\gamma_{\alpha_y}\eta_B(t)\\
-i\sum_k g_{\beta_x,k}\, e^{i(\omega_\beta-\omega_k)t}\,\eta_k(t) &= -\gamma_{\beta_x}\,\eta_X(t)\\
-ig_{\beta_y}\, e^{i(\omega_\beta-\omega_{c_y})t}\,\eta_q(t) &= -\gamma_{\beta_y}\,\eta_{Y,q}(t)
\end{aligned} \tag{A2}$$

Based on these formulas, a new form of the coupled equations of motion can be expressed as

$$\begin{aligned}
\dot\eta_B(t) &= -\gamma_{\alpha_x}\,\eta_B(t) - \gamma_{\alpha_y}\,\eta_B(t)\\
\dot\eta_X(t) &= -ig^*_{\alpha_x}\, e^{-i(\omega_\alpha-\omega_{c_x})t}\,\eta_B(t) - \gamma_{\beta_x}\,\eta_X(t)\\
\dot\eta_{Y,q}(t) &= -ig^*_{\alpha_y,q}\, e^{-i(\omega_\alpha-\omega_q)t}\,\eta_B(t) - \gamma_{\beta_y}\,\eta_{Y,q}(t)\\
\dot\eta_k(t) &= -ig^*_{\beta_x,k}\, e^{-i(\omega_\beta-\omega_k)t}\,\eta_X(t) - ig^{r*}_{x,1}\, e^{-i(\omega_{c_x}-\omega_{x,1})t}\,\eta^{ox}_k(t)\\
\dot\eta_q(t) &= -ig^r_{y,2}e^{i(\omega_{c_y}-\omega_{y,2})t}\,\eta^{oy}_q - ig^*_{\beta_y}e^{-i(\omega_\beta-\omega_{c_y})t}\,\eta_{Y,q}\\
\dot\eta^{ox}_k(t) &= -ig^{r*}_{x,1}e^{-i(\omega_{c_x}-\omega_{x,1})t}\,\eta_k - i\sum_l g^r_{x_l}e^{i(\omega_k-\omega_l)t}\,\eta^{ox}_l\\
\dot\eta^{oy}_q(t) &= -ig^{r*}_{y,2}e^{-i(\omega_{c_y}-\omega_{y,2})t}\,\eta_q - i\sum_m g^r_{y_m}e^{i(\omega_q-\omega_m)t}\,\eta^{oy}_m\\
\dot\eta^{ox}_l(t) &= -i\sum_k g^{r*}_{x_l}e^{-i(\omega_k-\omega_l)t}\,\eta^{ox}_k\\
\dot\eta^{oy}_m(t) &= -i\sum_q g^{r*}_{y_m}e^{-i(\omega_q-\omega_m)t}\,\eta^{oy}_q
\end{aligned} \tag{A3}$$

The amplitudes regarding the emissions inside and outside of the cavities are obtained by solving these ODEs in different steps in which the solutions for the first three equations are expressed as

$$\begin{aligned}
\eta_B(t) &= e^{-\gamma_\alpha t} \qquad \text{where} \quad \gamma_\alpha = \gamma_{\alpha_x}+\gamma_{\alpha_y}\\
\eta_X(t) &= ig^*_{\alpha_x}\frac{[e^{-i(\omega_\alpha-\omega_{c_x})t-\gamma_\alpha t}-e^{-\gamma_{\beta_x}t}]}{-i(\omega_\alpha-\omega_{c_x})+\gamma_{\beta_x}-\gamma_\alpha}\\
\eta_{Y,q}(t) &= ig^*_{\alpha_y,q}\frac{[e^{-i(\omega_\alpha-\omega_q)t-\gamma_\alpha t}-e^{-\gamma_{\beta_y}t}]}{-i(\omega_\alpha-\omega_q)+\gamma_{\beta_y}-\gamma_\alpha}
\end{aligned} \tag{A4}$$

Assuming $F_{X,k}(t) = ig^*_{\beta_x,k}\, e^{-i(\omega_\beta-\omega_k)t}\,\eta_X(t)$ and $F_{Y,q}(t) = ig^*_{\beta_y}e^{-i(\omega_\beta-\omega_{c_y})t}\,\eta_{Y,q}$ we arrive at,

$$\begin{aligned}
\eta_k(t) &= -\int_0^t \mathrm{d}t' F_{X,k}(t') - i\int_0^t \mathrm{d}t' g^{r*}_{x,1}\, e^{-i(\omega_{x,1}-\omega_{c_x})t'}\,\eta^{ox}_k(t')\\
\eta_q(t) &= -i\int_0^t \mathrm{d}t' g^r_{y,2}e^{i(\omega_{c_y}-\omega_2)t'}\,\eta^{oy}_q(t') - \int_0^t \mathrm{d}t' F_{Y,q}(t')
\end{aligned} \tag{A5}$$

We also define the following terms to simplify our equations for further analysis;

$$\begin{aligned} i\Omega_{k_\alpha} &= i\omega_{\alpha c_x} + i\omega_{\beta k} + \gamma_\alpha \\ i\Omega_{k_\beta} &= i\omega_{\beta k} + \gamma_{\beta_x} \\ i\Omega_{q_\alpha} &= i\omega_{\alpha q} + i\omega_{\beta c y} + \gamma_\alpha \\ i\Omega_{\beta} &= i\omega_{\beta c y} + \gamma_{\beta_y} \end{aligned} \tag{A6}$$

This helps us to obtain analytical solutions for the following amplitudes;

$$\begin{aligned} \eta_k^{ox}(t) = -i\frac{g_{x,1}^{r*} g_{\beta_x,k}^* g_{\alpha_x}^* e^{-\kappa_{x_l} t}}{-i(\omega_\alpha - \omega_{c_x}) + \gamma_{\beta_x} - \gamma_\alpha} \Bigg[& \frac{e^{-i\omega_{cx1}t - i\Omega_{k_\alpha}t + \kappa_{x_l}t} - 1}{-i\Omega_{k_\alpha}(-i\omega_{c_x 1} - i\Omega_{k_\alpha} + \kappa_{x_l})} - \frac{e^{-i\omega_{cx1}t + \kappa_{x_l}t} - 1}{-i\Omega_{k_\alpha}(-i\omega_{c_x 1} + \kappa_{x_l})} \\ & - \frac{e^{-i\omega_{cx1}t - i\Omega_{k_\beta}t + \kappa_{x_l}t} - 1}{-i\Omega_{k_\beta}(-i\omega_{c_x 1} - i\Omega_{k_\beta} + \kappa_{x_l})} + \frac{e^{-i\omega_{cx1}t + \kappa_{x_l}t} - 1}{-i\Omega_{k_\beta}(-i\omega_{c_x 1} + \kappa_{x_l})} \Bigg] \\ \eta_q^{oy}(t) = -i\frac{g_{y,2}^{r*} g_{\beta_y}^* g_{\alpha_y,q}^* e^{-\kappa_{y_m} t}}{-i(\omega_\alpha - \omega_q) + \gamma_{\beta_y} - \gamma_\alpha} \Bigg[& \frac{e^{-i\omega_{cy2}t - i\Omega_{q_\alpha}t + \kappa_{y_m}t} - 1}{-i\Omega_{q_\alpha}(-i\omega_{c_y 2} - i\Omega_{q_\alpha} + \kappa_{y_m})} - \frac{e^{-i\omega_{cy2}t + \kappa_{y_m}t} - 1}{-i\Omega_{q_\alpha}(-i\omega_{c_y 2} + \kappa_{y_m})} \\ & - \frac{e^{-i\omega_{cy2}t - i\Omega_{q_\beta}t + \kappa_{y_m}t} - 1}{-i\Omega_{\beta}(-i\omega_{c_y 2} - i\Omega_{\beta} + \kappa_{y_m})} + \frac{e^{-i\omega_{cy2}t + \kappa_{y_m}t} - 1}{-i\Omega_{\beta}(-i\omega_{c_y 2} + \kappa_{y_m})} \Bigg] \end{aligned} \tag{A7}$$

Here the decay rate of the intracavity modes[78,79] has been defined as;

$$\kappa_c = \pi \sum_i |g_i(\omega_c)|^2 = \frac{V}{\pi^2 c^3} \int_0^\infty \mathrm{d}\omega_i \; \omega_i^2 |g_i|^2$$

where the κ parameters are defined using equations similar to that above together with: $\omega_{ij} = \omega_i - \omega_j$, $\kappa_{x_l} = \kappa_1 + \kappa_l$ and $\kappa_{y_m} = \kappa_2 + \kappa_m$. This leads to an expression for the amplitude of the outgoing waves as follows:

$$\eta_l^{ox} = -i\frac{\omega_l^2 g_{x_l}^{r*} V}{\pi^2 c^3} \int_0^t \mathrm{d}t' \int_0^\infty e^{-i(\omega_k - \omega_l)t'} \eta_k^{ox}(t') \mathrm{d}\omega_k \tag{A8a}$$

$$\eta_l^{ox} \approx -\frac{4\omega_l^2 V}{\pi c^3} \frac{g_{x_l}^{r*} g_{x,1}^{r*} g_{\beta_x,k}^* g_{\alpha_x}^*}{(\omega_{c_x 1} + i\kappa_{x_l})(-i\omega_{\beta l} - i\omega_{c_x 1} - i\omega_{\alpha c_x} - \gamma_\alpha)(-i\omega_{\beta l} - i\omega_{c_x 1} - \gamma_{\beta x})} \tag{A8b}$$

$$\approx -2 g_{\beta_x}^* g_{\alpha_x}^* \frac{\kappa_{x_l}}{(\omega_{c_x 1} + i\kappa_{x_l})(-i\omega_{\beta l} - i\omega_{c_x 1} - i\omega_{\alpha c_x} - \gamma_\alpha)(-i\omega_{\beta l} - i\omega_{c_x 1} - \gamma_{\beta x})} \tag{A8c}$$

$$\eta_m^{oy} = -i\Big(\frac{\omega_m^2 g_{y_m}^{r*} V}{\pi^2 c^3}\Big) \int_0^t \mathrm{d}t' \int_0^\infty \mathrm{d}\omega_q \, e^{-i(\omega_q - \omega_m)t'} \eta_q^{oy}(t') \mathrm{d}\omega_q \tag{A9a}$$

$$\eta_m^{oy} \approx -\Big(2\frac{\omega_m^2 V}{\pi c^3}\Big) \frac{g_{y_m}^{r*} g_{y,2}^{r*} g_{\beta_y}^* g_{\alpha_y,q}^*}{(\omega_{c_y 2} + i\kappa_{y_m})(-i\omega_{\alpha m} - i\omega_{\beta c_y} - i\omega_{c_y 2} - \gamma_\alpha)(-i\omega_{\beta c_y} - \gamma_{\beta_y})} \tag{A9b}$$

$$\approx -g_{\beta_y}^* g_{\alpha_y}^* \frac{\kappa_{y_m}}{(\omega_{c_y 2} + i\kappa_{y_m})(-i\omega_{\alpha m} - i\omega_{\beta c_y} - i\omega_{c_y 2} - \gamma_\alpha)(-i\omega_{\beta c_y} - \gamma_{\beta_y})} \tag{A9c}$$

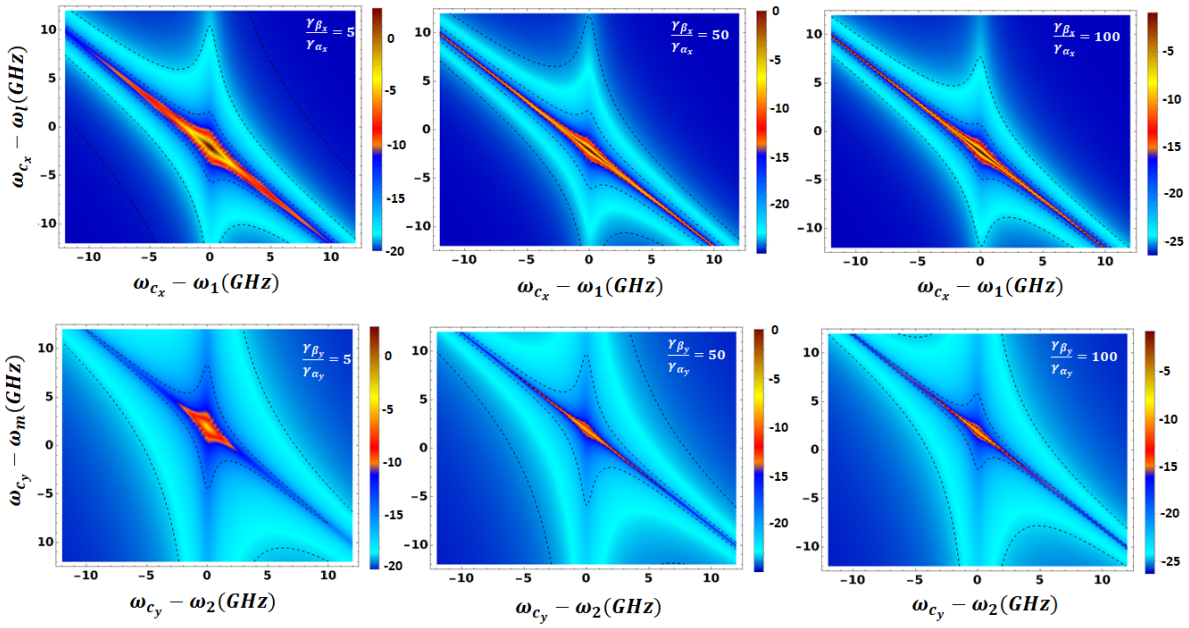

FIG. 8. For different ratios of $\gamma_{\beta_{x/y}}$ to $\gamma_{\alpha_{x/y}}$, we show the joint spectral density. Top panel; $|\eta_l^{ox}|^2$ and bottom panel; $|\eta_m^{oy}|^2$. Here we choose $|\omega_\alpha - \omega_{c_x}| = |\omega_\beta - \omega_{c_y}| = 0.05$ GHz, $\omega_\alpha = 1.5$ GHz, $\omega_\beta = 3.5$ GHz, $\phi = \pi/4$, $\kappa_{x_l} = \kappa_{y_m} = 0.5$ GHz. The scale bar is logarithmic and the dashed lines(-16 to -6 with stepping of 5) refer to the same intensity scale for X and Y polarization direction.

Here we assumed that $g_{\beta_x,k} \approx g_{\beta_x}$, $g_{\alpha_y,q} \approx g_{\alpha_y}$, $g^r_{x_l} \approx g^r_{x,1}$ and $g^r_{y_m} \approx g^r_{y,2}$. The above analytical expression are related to Eq. 7 and 8 in main text. It is to be noted, in solving the above system, where needed, we changed the sum into an integral over frequency as follows,

$$\sum_j \to 2\frac{V}{(2\pi)^3}\int_0^{2\pi} \mathrm{d}\phi' \int_0^{\pi} \mathrm{d}\theta \sin\theta \int_0^{\infty} \mathrm{d}k_j\, k_j^2 = \frac{V}{\pi^2 c^3}\int_0^{\infty} \mathrm{d}\omega_j\, \omega_j^2 \tag{A10}$$

Also, we have taken the long time limit in evaluating these equations.

Appendix B: Toward Schmidt analysis

Schmidt decomposition is a unique mathematical method for characterising a bipartite system in terms of a complete set of basis states. As a result of this decomposition, one can calculate the Schmidt number, which defines the "degree" of entanglement for the two-photon state[80–82]. Previously, we have shown[51] an analytical expression for the Schmidt number of the cascade emitters which has a strong dependence on the ratio of decay rates of the first and second photons. Here although we didn't formulate the Schmidt number for the current system, we observe the

strong dependence of our system on the ratio of $\gamma_{\beta_{x/y}}/\gamma_{\alpha_{x/y}}$. In Fig. 8 we show how the joint spectral density is differentiated when ratio of $\gamma_{\beta_{x/y}}$ to $\gamma_{\alpha_{x/y}}$ varies. The top panel relates to $|\eta_l^{ox}|^2$ and bottom panel shows results for $|\eta_m^{oy}|^2$. From the JSD here, we may conclude that the frequency correlation which is related to the degree of entanglement of states of the two-photons depends on the emission decay ratios, however, for a QD-cavity system there might be other characteristic parameters of the system playing role.

DATA AVAILABILITY

The data that support the findings of this study are available from the corresponding author upon reasonable request.

REFERENCES

[1]W. B. Gao, A. Imamoglu, H. Bernien, and R. Hanson, Nature Photonics **9**, 363 (2015).

[2]A. F. Koenderink, A. Alu, and A. Polman, Science **348**, 516–521 (2015).

[3]C. Yi and E. Crosson, npj Quantum Information **8**, 37 (2022).

[4]C. S. Hamilton, R. Kruse, L. Sansoni, S. Barkhofen, C. Silberhorn, and I. Jex, Phys. Rev. Lett. **119**, 170501 (2017).

[5]V. Giovannetti, S. Lloyd, and L. Maccone, Nat. Photon **5**, 222 (2011).

[6]H. P. Specht, C. Nölleke, A. Reiserer, M. Uphoff, E. Figueroa, S. Ritter, and G. Rempe, Nature **473**, 190 (2011).

[7]J. I. Cirac, P. Zoller, H. J. Kimble, and H. Mabuchi, Phys. Rev. Lett. **78**, 3221 (1997).

[8]L. L. Lau and S. Dutta, Phys. Rev. Research **4**, L012007 (2022).

[9]T. K. Paraïso, T. Roger, D. G. Marangon, I. De Marco, M. Sanzaro, R. I. Woodward, J. F. Dynes, Z. Yuan, and A. J. Shields, Nature Photonics **15**, 850 (2021).

[10]A. Eich, T. C. Spiekermann, H. Gehring, L. Sommer, J. R. Bankwitz, P. P. J. Schrinner, J. A. Preub, S. Michaelis de Vasconcellos, R. Bratschitsch, W. H. P. Pernice, and C. Schuck, ACS Photonics **9**, 551 (2022).

[11]I. Aharonovich, D. Englund, and M. Toth, Nature Photonics **10**, 631 (2016).

[12]D. A. Vajner, L. Rickert, T. Gao, K. Kaymazlar, and T. Heindel, Advanced Quantum Technologies **5**, 2100116 (2022).

[13]C.-Y. Lu and J.-W. Pan, Nature Nanotechnology **16**, 1294 (2021).

[14]P. Lodahl, Quantum Science and Technology **3**, 013001 (2017).

[15]P. Lodahl, S. Mahmoodian, and S. Stobbe, Rev. Mod. Phys. **87**, 347 (2015).

[16]X. Ding, Y. He, Z.-C. Duan, N. Gregersen, M.-C. Chen, S. Unsleber, S. Maier, C. Schneider, M. Kamp, S. Höfling, C.-Y. Lu, and J.-W. Pan, Phys. Rev. Lett. **116**, 020401 (2016).

[17]C. R. Kagan, L. C. Bassett, C. B. Murray, and S. M. Thompson, Chem. Rev. **121**, 3186 (2021).

[18]P. P. J. Schrinner, J. Olthaus, D. E. Reiter, and C. Schuck, Nano Lett. **20**, 8170 (2020).

[19]H. Lu, G. M. Carroll, N. R. Neale, and M. C. Beard, ACS Nano **13**, 939 (2019).

[20]C. Monroe, D. M. Meekhof, B. E. King, and D. J. A. Wineland, Science **272**, 1131–1136 (1996).

[21]L. Slodička, G. Hétet, N. Röck, P. Schindler, M. Hennrich, and R. Blatt, Phys. Rev. Lett. **110**, 083603 (2013).

[22]K. De Greve, L. Yu, P. L. McMahon, J. S. Pelc, C. M. Natarajan, N. Y. Kim, E. Abe, S. Maier, C. Schneider, M. Kamp, S. Höfling, R. H. Hadfield, A. Forchel, M. M. Fejer, and Y. Yamamoto, Nature **491**, 421 (2012).

[23]P. A. Michler, Science **290**, 2282–2285 (2000).

[24]I. Schwartz, D. Cogan, E. R. Schmidgall, Y. Don, L. Gantz, O. Kenneth, N. H. Lindner, and D. Gershoni, Science **354**, 434 (2016).

[25]J.-C. Besse, K. Reuer, M. C. Collodo, A. Wulff, L. Wernli, A. Copetudo, D. Malz, P. Magnard, A. Akin, M. Gabureac, G. J. Norris, J. I. Cirac, A. Wallraff, and C. Eichler, Nature Communications **11**, 4877 (2020).

[26]S. C. Wein, J. C. Loredo, M. Maffei, P. Hilaire, A. Harouri, A. Lemaître, I. Sagnes, L. Lanco, O. Krebs, A. Auffèves, C. Simon, P. Senellart, and C. Antón-Solanas, Nature Photonics (2022).

[27]C.-M. Lee, H.-J. Lim, C. Schneider, S. Maier, S. Höfling, M. Kamp, and Y.-H. Lee, Scientific Reports **5**, 14309 (2015).

[28]K. J. Vahala, Nature **424**, 839 (2003).

[29]M. Schwab, H. Kurtze, T. Auer, T. Berstermann, M. Bayer, J. Wiersig, N. Baer, C. Gies, F. Jahnke, J. P. Reithmaier, A. Forchel, M. Benyoucef, and P. Michler, Phys. Rev. B **74**, 045323 (2006).

[30]K. Srinivasan, P. E. Barclay, O. Painter, J. Chen, A. Y. Cho, and C. Gmachl, Applied Physics Letters **83**, 1915 (2003).

[31]F. Liu, A. J. Brash, J. O'Hara, L. M. P. P. Martins, C. L. Phillips, R. J. Coles, B. Royall, E. Clarke, C. Bentham, N. Prtljaga, I. E. Itskevich, L. R. Wilson, M. S. Skolnick, and A. M. Fox, Nature

Nanotechnology **13**, 835–840 (2018).

[32]O. Iff, Q. Buchinger, M. Moczała-Dusanowska, M. Kamp, S. Betzold, M. Davanco, K. Srinivasan, S. Tongay, C. Anton-Solanas, S. Höfling, and C. Schneider, Nano Letters **21**, 4715 (2021).

[33]A. Nunnenkamp, K. Børkje, and S. M. Girvin, Phys. Rev. A **85**, 051803 (2012).

[34]L. Sapienza, M. Davanço, A. Badolato, and K. Srinivasan, Nature Communications **6**, 7833 (2015).

[35]M. Gschrey, A. Thoma, P. Schnauber, M. Seifried, R. Schmidt, B. Wohlfeil, L. Krüger, J. H. Schulze, T. Heindel, S. Burger, F. Schmidt, A. Strittmatter, S. Rodt, and S. Reitzenstein, Nature Communications **6**, 7662 (2015).

[36]T. Herzog, S. Böhrkircher, S. Both, M. Fischer, R. Sittig, M. Jetter, S. L. Portalupi, T. Weiss, and P. Michler, Phys. Rev. B **102**, 235306 (2020).

[37]D. Najer, I. Söllner, P. Sekatski, V. Dolique, M. C. Löbl, D. Riedel, R. Schott, S. Starosielec, S. R. Valentin, A. D. Wieck, N. Sangouard, A. Ludwig, and R. J. Warburton, Nature **575**, 622 (2019).

[38]F. Li, Y. Li, Y. Cai, P. Li, H. Tang, and Y. Zhang, Advanced Quantum Technologies **2**, 1900060 (2019).

[39]T. Herzog, M. Sartison, S. Kolatschek, S. Hepp, A. Bommer, C. Pauly, F. Mücklich, C. Becher, M. Jetter, S. L. Portalupi, and P. Michler, Quantum Science and Technology **3**, 034009 (2018).

[40]D. Najer, M. Renggli, D. Riedel, S. Starosielec, and R. J. Warburton, Applied Physics Letters **110**, 011101 (2017).

[41]L. Greuter, S. Starosielec, A. V. Kuhlmann, and R. J. Warburton, Phys. Rev. B **92**, 045302 (2015).

[42]K. A. Atlasov, K. F. Karlsson, A. Rudra, B. Dwir, and E. Kapon, Opt. Express **16**, 16255 (2008).

[43]A. Dousse, J. Suffczyński, A. Beveratos, O. Krebs, A. Lemaître, I. Sagnes, J. Bloch, P. Voisin, and P. Senellart, Nature **466**, 217 (2010).

[44]M. Benyoucef, J.-B. Shim, J. Wiersig, and O. G. Schmidt, Opt. Lett. **36**, 1317 (2011).

[45]S. Seyfferle, F. Hargart, M. Jetter, E. Hu, and P. Michler, Phys. Rev. B **97**, 035302 (2018).

[46]T. Heindel, A. Thoma, M. von Helversen, M. Schmidt, A. Schlehahn, M. Gschrey, P. Schnauber, J. H. Schulze, A. Strittmatter, J. Beyer, S. Rodt, A. Carmele, A. Knorr, and S. Reitzenstein, Nature Communications **8**, 14870 (2017).

[47]L. Schweickert, K. D. Jöns, K. D. Zeuner, S. F. Covre da Silva, H. Huang, T. Lettner, M. Reindl, J. Zichi, R. Trotta, A. Rastelli, and V. Zwiller, Applied Physics Letters **112**, 093106 (2018).

[48]R. Winik, D. Cogan, Y. Don, I. Schwartz, L. Gantz, E. R. Schmidgall, N. Livneh, R. Rapaport, E. Buks, and D. Gershoni, Phys. Rev. B **95**, 235435 (2017).

[49]R. Trotta, J. S. Wildmann, E. Zallo, O. G. Schmidt, and A. Rastelli, Nano Letters **14**, 3439 (2014).

[50]K. N. Avanaki and G. C. Schatz, The Journal of Physical Chemistry Letters **10**, 3181 (2019).

[51]K. N. Avanaki and G. C. Schatz, The Journal of Chemical Physics **154**, 024304 (2021).

[52]R. Keil, M. Zopf, Y. Chen, B. Höfer, J. Zhang, O. G. Schmidt, F. Ding, and O. G. Schmidt, Nature Communications **8**, 15501 (2017).

[53]D. Huber, M. Reindl, Y. Huo, H. Huang, J. S. Wildmann, O. G. Schmidt, A. Rastelli, and R. Trotta, Nature Communications **8**, 15506 (2017).

[54]K. Edamatsu, Japan Society of Applied Physics **46**, 7175 (2007).

[55]T. Moradi, M. B. Harouni, and M. H. Naderi, Phys. Rev. A **96**, 023836 (2017).

[56]O. Benson, C. Santori, M. Pelton, and Y. Yamamoto, Phys. Rev. Lett. **84**, 2513 (2000).

[57]M. Zieliński, Scientific Reports **10**, 13542 (2020).

[58]C. Santori, D. Fattal, M. Pelton, G. S. Solomon, and Y. Yamamoto, Phys. Rev. B **66**, 045308 (2002).

[59]T. M. Stace, G. J. Milburn, and C. H. W. Barnes, Phys. Rev. B **67**, 085317 (2003).

[60]R. M. Stevenson, R. J. Young, P. Atkinson, K. Cooper, R. D. A., and A. J. Shields, Nature **439**, 179–182 (2006).

[61]B. D. Gerardot, S. Seidl, P. A. Dalgarno, R. J. Warburton, D. Granados, J. M. Garcia, K. Kowalik, O. Krebs, K. Karrai, A. Badolato, and P. M. Petroff, Applied Physics Letters **90**, 041101 (2007).

[62]R. Singh and G. Bester, Phys. Rev. Lett. **104**, 196803 (2010).

[63]N. Akopian, N. H. Lindner, E. Poem, Y. Berlatzky, J. Avron, D. Gershoni, B. D. Gerardot, and P. M. Petroff, Phys. Rev. Lett. **96**, 130501 (2006).

[64]P. K. Pathak and S. Hughes, Phys. Rev. B **80**, 155325 (2009).

[65]P. K. Pathak and S. Hughes, Phys. Rev. B **79**, 205416 (2009).

[66]A. Borne, T. E. Northup, R. Blatt, and B. Dayan, Opt. Express **28**, 11822 (2020).

[67]S. E. Ulloa, E. Sun, D. Feng, and T. Jia, Advances in Condensed Matter Physics **2014**, 219381 (2014).

[68]M. B. . E. Wolf, *Principles of Optics* (Cambridge University, 1999) pp. 287–302.

[69]H. Wang, H. Hu, T.-H. Chung, J. Qin, X. Yang, J.-P. Li, R.-Z. Liu, H.-S. Zhong, Y.-M. He, X. Ding, Y.-H. Deng, Q. Dai, Y.-H. Huo, S. Höfling, C.-Y. Lu, and J.-W. Pan, Phys. Rev. Lett. **122**, 113602 (2019).

[70]Y. Chen, M. Zopf, R. Keil, F. Ding, and O. G. Schmidt, Nature Communications **9** (2018).

[71]C. S. Muñoz, F. P. Laussy, C. Tejedor, and E. del Valle, New Journal of Physics **17**, 123021 (2015).

[72]E. del Valle, New Journal of Physics **15**, 025019 (2013).

[73]R. J. Young, R. M. Stevenson, P. Atkinson, K. Cooper, D. A. Ritchie, and A. J. Shields, New Journal of Physics **8**, 29 (2006).

[74]R. M. Stevenson, R. J. Young, P. Atkinson, K. Cooper, R. A., and A. J. Shields, Nature **439**, 179–182 (2006).

[75]K. E. Dorfman, B. Asban, Shahaf aand Gu, and S. Mukamel, Communications Physics **4**, 49 (2021).

[76]H. Kim, S. M. Lee, O. Kwon, and H. S. Moon, Scientific Reports **7**, 5772 (2017).

[77]J. Z. Lin, K. Hou, C. J. Zhu, and Y. P. Yang, Phys. Rev. A **99**, 053850 (2019).

[78]G. Cui and M. G. Raymer, Phys. Rev. A **73**, 053807 (2006).

[79]H. J. Carmichael, *Statistical Methods in Quantum Optics 1* (Springer, New York, 1999) pp. 287–302.

[80]C. K. Law, I. A. Walmsley, and J. H. Eberly, Phys. Rev. Lett. **84**, 5304 (2000).

[81]J. H. Eberly, Laser Physics **16**, 921 (2006).

[82]C. Chen, C. Bo, M. Y. Niu, F. Xu, Z. Zhang, J. H. Shapiro, and F. N. C. Wong, Opt. Express **25**, 7300 (2017).